# Reliable Joint Segmentation of Retinal Edema Lesions in OCT Images

Meng Wang, Kai Yu, Chun-Mei Feng, Ke Zou, Yanyu Xu, Qingquan Meng, Rick Siow Mong Goh, Yong Liu, Xinxing Xu, and Huazhu Fu



**Abstract**—Focusing on the complicated pathological features, such as blurred boundaries, severe scale differences between symptoms, background noise interference, etc., in the task of retinal edema lesions joint segmentation from OCT images and enabling the segmentation results more reliable. In this paper, we propose a novel reliable multi-scale wavelet-enhanced transformer network, which can provide accurate segmentation results with reliability assessment. Specifically, aiming at improving the model's ability to learn the complex pathological features of retinal edema lesions in OCT images, we develop a novel segmentation backbone that integrates a wavelet-enhanced feature extractor network and a multi-scale transformer module of our newly designed. Meanwhile, to make the segmentation results more reliable, a novel uncertainty segmentation head based on the subjective logical evidential theory is introduced to generate the final segmentation results with a corresponding overall uncertainty evaluation score map. We conduct comprehensive experiments on the public database of AI-Challenge 2018 for retinal edema lesions segmentation, and the results show that our proposed method achieves better segmentation accuracy with a high degree of reliability as compared to other state-of-the-art segmentation approaches. The code will be released on: https://github.com/LooKing9218/ReliableRESeg.

**Index Terms**—Reliable segmentation, Multi-scale transformer, Wavelet, Retinal edema lesions

## 1 Introduction

Retinal edema lesions are highly correlated symptoms of diabetic retinopathy (DR) including the symptoms of retina edema (RE), sub-retinal fluid (SRF), and pigment epithelial detachment (PED) [1]. Retinal optical coherence tomography (OCT) is a non-invasive imaging technology that can visualize the cross-sectional structure of the retina, and it has been widely used in the diagnosis of retinal diseases [2]. Ophthalmologists can evaluate retinal edema lesions efficiently through retinal OCT images [3]. Therefore, accurate segment retinal edema lesions from OCT images can greatly aid ophthalmologists in evaluating diseases and specifying treatment plans [4]. Recently, many segmentation methods based on the convolutional neural networks (CNNs) [5]–[8] have been proposed. While these CNN-based methods achieved excellent performance, there is a limitation in modeling explicit long-range dependent global features due to the inherent locality of convolutional operations. Focusing on this limitation, many studies attempted to introduce the transformer to improve the model's ability to learn long-range dependent global information [9], [10]. And, several transformer-based segmentation models have also been proposed for image segmentation and achieved comparable performance with CNN-based approaches [11]–[13]. However, few previous studies have explored the challenges in the task of retinal edema lesions joint segmentation from OCT images. As shown in Fig. 1, retinal edema lesions in OCT images have some specific challenging characteristics, such as PEDs usually occupy a small proportion of the whole OCT image, which may cause the loss of small-size feature information during down-sampling, resulting in a decrease in the segmentation accuracy of PEDs. In contrast to PEDs, RE and SRF always have larger sizes, but they usually show large morphological differences in different OCT slices, and RE is always characterized by blurred borders, which leads to performance degradation for the segmentation methods designed for other tasks. In addition, most previous segmentation methods mainly focus on the improvement of segmentation accuracy, ignoring the assessment for the reliability of segmentation results, which leads to unreliability when deployed in evidence-critical retinal disease evaluation applications. In summary, there are still three main challenges in the task of retinal edema lesions joint segmentation from OCT images: 1) How to avoid the loss of small-sized features during down-sampling, while enhancing the model's ability to represent local detailed features, such as retinal structure information and tiny PED lesion features. 2) How to improve the ability of the model to learn complex multi-scale global semantic information of retinal edema lesions in OCT images. 3) How to evaluate

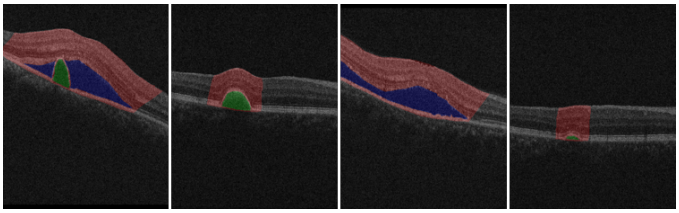

Fig. 1. Examples of retinal edema lesions. Red, blue, and green represent RE, SRF, and PED, respectively.


- *Meng Wang and Kai Yu contributed equally to this work. Corresponding author: Huazhu Fu (hzfu@ieee.org).*
- *Meng Wang, Kai Yu, Chun-Mei Feng, Yanyu Xu, Rick Siow Mong Goh, Yong Liu, Xinxing Xu, and Huazhu Fu are with institute of high performance computing, agency for science, technology and research (A*STAR), Singapore 138632, Singapore.*
- *Ke Zou is with National Key Laboratory of Fundamental Science on Synthetic Vision and the College of Computer Science, Sichuan University, Chengdu 610065, China.*
- *Qingquan Meng is with Soochow University, Suzhou 215006, China.*

the confidence of the segmentation results to make the segmentation results reliable without accuracy loss.

Therefore, in this paper, we propose a novel reliable multi-scale wavelet-enhanced transformer network focusing on these challenges in the task of retinal edema lesions joint segmentation from OCT images. **Our main contributions of this paper can be summarized as follows:**

- We design a novel feature extractor network by replacing the down-sampling operation in pre-trained ResNet with our newly proposed adaptive wavelet down-sampling (AWDS) module, which can generate a wavelet representation to avoid small feature loss while enhancing the ability of the network to represent local multi-resolution detailed features.
- A novel multi-scale transformer (AMsTrans) module is developed to combine with our proposed wavelet-enhanced feature extractor network, which aims to further improve the model's capacity of extracting the multi-scale long-range dependent global features of the retinal edema lesions.
- To make the segmentation results more reliable, an uncertainty-aware segmentation head based on the subjective logic evidence theory is introduced to generate the final segmentation result for retinal edema lesions, while giving a corresponding overall uncertainty evaluation score map to evaluate the confidence of the segmentation result without accuracy loss.
- We conduct comprehensive experiments on the public database of AI-Challenge 2018 for retinal edema lesions segmentation, and the results show that our proposed method outperforms other state-of-the-art segmentation approaches. Meanwhile, with the estimated uncertainty, our method could produce a reliable segmentation result, and potentially avoid disasters from out-of-distribution (OOD) samples.

## 2 Related Works

**Image segmentation methods based on CNN:** Deep learning especially for the convolutional neural networks (CNNs) has been demonstrated with highly feature representations that have achieved excellent performance in many computer vision tasks [14]–[18]. Recently, numerous end-to-end CNN-based segmentation methods have been proposed and achieved promising performance [5]–[8], [19], [20]. Currently, the CNN-based methods can be summarized as two architectures: fully convolutional network (FCN) architecture [19]–[21] and U-shaped (UNet) framework [5]–[8], [22]. Usually, the FCN architecture uses a classic baseline model such as VGG [15] or ResNet [17] as the backbone network to extract the rich semantic information of the input data, and then directly restore the top-level features to the input image size to segment the target. The segmentation approaches based on the U-shaped architecture is mainly composed of three core components: an encoder for extracting rich features of the input image, a decoder for gradually restoring the resolution information of the top-level features, and skip-connection to fuse the information from different levels of the encoder with the corresponding decoder's features. Although these CNN-based methods have achieved promising results in their respective specific segmentation tasks, the direct application of these methods to the segmentation of retinal edema lesions in OCT images still suffers from two limitations: 1) Simple down-sampling operations often result in the loss of feature information of small lesions, leading to low segmentation accuracy of tiny PED lesions with very small regional proportions. 2) These methods are incapable of modeling explicit long-range global features due to the inherent locality of convolution operations.

**Image segmentation methods based on Transformer:** The transformer was originally proposed for modeling the long-range dependent information of timing signals in natural language processing (NLP) tasks [9]. With the impressive achievements of Transformer in the field of NLP [23]–[25], researchers have extended it to the field of computer vision [10]. Recently, transformer-based methods [13], [26], [27] have also achieved comparable performance to CNNs in many vision tasks as the transformer layer has unlimited receptive fields and can capture long-range dependency global features. Several segmentation methods based on transformer have also been proposed for medical image segmentation [11], [12], [28]. However, the performance of these methods in the task of retinal edema lesions segmentation with complex pathological features is degraded due to the weaker local detail feature representation ability of the transformer. In addition, most of these methods explore long-range dependent features at a single scale, which is another important reason for the performance degradation when these methods are applied to the segmentation of retinal edema lesions with complex scale features. Therefore, how to improve the ability of the model to learn complex multi-scale global contextual information of retinal edema lesions is crucial for improving the segmentation performance of the model. Recently, some previous works have improved the model's ability to represent multi-scale global features by introducing a multi-scale learning module when designing the model. [29] proposed CoTr for accurate 3D medical image segmentation. Under this framework, the CNN is constructed to extract feature representations and an efficient deformable Transformer (DeTrans) is built to model the long-range dependency on the extracted feature maps. [30] designed M2TR to capture the subtle manipulation artifacts at different scales using transformer models. [31] introduced adaptive attention multi-scale fusion transformer (AFTrans) to capture region attention without box annotations and compensate for ViT shortcomings in fine-grained visual recognition. However, most previous multi-scale methods still approach exploring multi-scale features in a specified-sized feature map, ignoring the exploration with different sizes and different semantic information. Different from previous multi-scale approaches [8], [29]–[31], our proposed multi-scale transformer module explores the multi-scale features by adaptively aggregating the global long-dependent information in multi-scale feature maps from different levels of feature extractor network.

**Wavelet for local detailed feature information representation:** Wavelet transform has a good local detailed feature representation capacity in the time-frequency domain, and can present any local details in the image, so it is widely used to deal with various image problems [32]–[34]. Inspired by the resemblance between multi-resolution analysis and the convolutional filtering and pooling opera-

tions in CNNs, there are several previous works dedicated to developing wavelet convolutional neural networks for computer vision tasks [35]–[37]. Although the Wavelet network can model local multi-resolution detail features well, compared to the classic CNN-based baseline models such as ResNet [17] and DenseNet [38], their ability to learn complex texture features of images is weak. Therefore, enhancing the model's ability to learn complex texture features of images is crucial for applying wavelet theory to the joint segmentation task of retinal edema lesions from OCT images. Therefore, in this paper, we construct the feature extractor network to explore local multi-resolution detailed features by integrating our proposed adaptive wavelet down-sampling module with the pre-trained ResNet blocks.

**Uncertainty-based learning:** the past decade, deep learning-based methods have achieved tremendous excellent results in various CV tasks [10], [13], [14], [16]–[18]. However, these deep learning models are essentially deterministic functions and thus cannot provide uncertainty estimation for final decisions. Therefore, the uncertainty learning method has gradually attracted the attention of researchers. Bayesian Neural Networks (BNNs) [39]–[41] obtain deep model uncertainty by substituting model deterministic weight parameters. However, BNNs usually come with a high computational cost, therefore, Gal et al [42]. proposed a more scalable and practical approach, MC-dropout, in which the inference decision is obtained by dropout sampling of weights during training and testing. Lakshminarayanan et al [43]. proposed ensemble-based uncertainty methods by training and integrating multiple deep networks, which also achieved promising performance. Unlike these methods to obtain uncertainty estimation by modeling uncertainty through network weights, Sensoy et al [44]. proposed an uncertainty method based on the subjective logical evidential theory that directly models uncertainty without ensemble or Monte Carlo sampling. Building upon RBF networks, Amersfoort et al [45]. adopted the distance between test samples and prototypes as the agency for deterministic uncertainty. Furthermore, Han et al [46]. proposed a unified multi-view uncertainty classification method by combining subjective logical theory with the Dirichlet distribution, which achieved excellent performance in the task of multi-view classification. However, unlike the previous studies on single/multi-view classification, our joint segmentation task for retinal edema lesions is not a simple classification task, and it also needs to consider the spatial continuity of the lesion area to give high uncertainty scores to incorrect segmented regions.

## 3 METHODS

### 3.1 Overall architecture

As shown in Fig. 2, our proposed reliable multi-scale wavelet-enhanced transformer network is designed based on the U-shaped architecture that mainly consists of four components: the wavelet-enhanced feature extractor network which integrates the pre-trained ResNet blocks with our proposed adaptive wavelet down-sampling (AWDS) module, it aims to extract the complicated feature information in the retinal OCT image; the AMsTrans module is appended on the top layer of feature extractor network to guide the model to explore the multi-scale long-range dependent global features of retinal lesions; the decoder path to restore the spatial information with strong multi-scale global features generated by AMsTrans module and gradually fuse the multi-semantic contextual information from different stages of feature extractor network; the uncertainty-aware segmentation head is adapted to generate the final segmentation results with corresponding uncertainty score map, where regions with high uncertainty scores indicate that the segmentation result in that region may be incorrect and may require double-check by the physician, while regions with low certainty scores indicate a high level of confidence in the segmentation result.

### 3.2 Wavelet-enhanced feature extractor network

As shown in Fig. 3, to extract the complex feature information in OCT images while enhancing the model's ability to extract the local multi-resolution detailed information, we propose a novel feature extractor network, which mainly consists of the pre-trained ResNet blocks and AWDS module.

Previous studies have shown that pre-trained ResNet has good feature representation capability and is widely used as a feature extraction backbone in different vision tasks [7], [8], [19]. While these methods have achieved remarkable performance, they are essentially spatial approaches and usually ignore spectral information that is crucial for representing the multi-resolution local detailed features in OCT images. In addition, the down-sampling operation in ResNet may also result in the loss of small-sized symptomatic features of retinal edema lesions, leading to poor segmentation performance for PEDs with small-size features. Furthermore, it has been demonstrated that wavelet transform has a good local multi-resolution detailed feature representation capacity in the time-frequency domain, thus can present any local details in the image [32], [34], [35], [37].

Therefore, we introduce wavelet theory and develop a novel AWDS module to replace the down-sampling operation in ResNet, which can supplement the missing spectral information in ResNet and improve the model's ability to extract local multi-resolution detailed features. The architecture of the proposed AWDS module is shown in Fig. 3. In AWDS module, we adopt 2D adaptive lifting scheme to perform multi-resolution wavelet transform on the input feature maps **Input** $\in \mathrm{R}^{(C,H,W)}$ to generate four wavelet sub-bands feature maps (**LL** $\in \mathrm{R}^{(C,H/2,W/2)}$, **LH** $\in \mathrm{R}^{(C,H/2,W/2)}$, **HL** $\in \mathrm{R}^{(C,H/2,W/2)}$, and **HH** $\in \mathrm{R}^{(C,H/2,W/2)}$), and a Conv3×3 operation is used to fuse the features of different sub-bands to achieve down-sampling without any feature loss.

#### 3.2.1 *The adaptive horizontal lifting scheme*

The input 2D feature map is first split into the even ($I_e\left[n,:\right] = I\left[2n,:\right]$) and odd ($I_o\left[n,:\right] = I\left[2n+1,:\right]$) horizontal components. Then, a horizontal updater ($U_h$) and a horizontal predictor ($P_h$) are performed on the split components to generate the approximation $L_H$ and the details $H_H$ sub-bands of the wavelet transformation as follows,

$$\begin{aligned} L_H\left[n,:\right] &= I_e\left[n,:\right] + \mathrm{U_h}\left(I_o\left[n,:\right]\right), \\ H_H\left[n,:\right] &= I_o\left[n,:\right] - P_h\left(L_H\left[n,:\right]\right), \end{aligned} \tag{1}$$

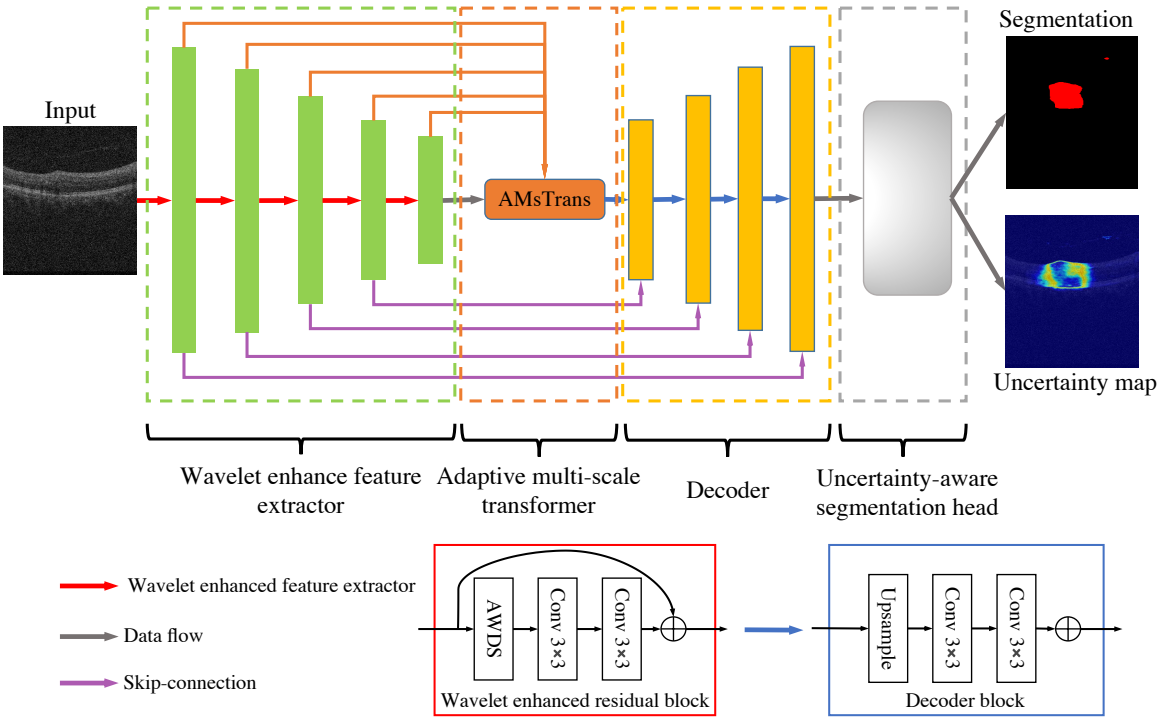


Fig. 2. The framework of our proposed reliable multi-scale wavelet enhanced transformer network. Our proposed method mainly consists of four components: a novel wavelet-enhanced feature extractor network which integrates the pre-trained ResNet blocks with our proposed adaptive wavelet down-sampling (AWDS) module, it aims to extract the complicated feature information in the retinal OCT image; the adaptive multi-scale transformer (AMsTrans) module is appended on the top layer of feature extractor network to guide the model to explore the multi-scale long-range dependent global features of retinal lesions; the decoder path to restore the spatial information with strong multi-scale global features generated by AMsTrans module and gradually fuse the multi-semantic contextual information from different stages of feature extractor network; the uncertainty-aware segmentation head is used to generate the final segmentation results with corresponding uncertainty score map, where regions with high uncertainty scores indicate that the segmentation result in that region may be incorrect and may require double-check by the physician, while regions with low certainty scores indicate a high level of confidence in the segmentation result.

where $U_h$ and $P_h$ are two learnable blocks consisting of convolutional operations as shown in Fig.3, both of which can adaptively optimize their coefficients during training by gradient back-propagation.

### 3.2.2 *The adaptive vertical lifting scheme*

Similar to the adaptive horizontal lifting scheme, take $H_H$ as an example, the input 2D feature map $H_H$ is first split into the even ($H_{He}[:,n] = H_H[:,2n]$) and odd ($H_{Ho}[:,n] = H_H[:,2n+1]$) vertical components. Then, a vertical updater ($U_v$) and a vertical predictor ($P_v$) are performed on the split components to generate the approximation $HH$ and the details $HL$ sub-bands of the wavelet transformation as follows,

$$\begin{aligned} HL[:,n] &= H_{He}[n,:] + \mathrm{U_v}\left(H_{Ho}[n,:]\right), \\ HH[:,n] &= H_{Ho}[n,:] - P_v\left(HL[n,:]\right). \end{aligned} \tag{2}$$

Like $U_h$ and $P_h$, both $U_v$ and $P_v$ are also learnable blocks consisting of convolutional operations as shown in Fig. 3, both of which can adaptively optimize their coefficients during training by gradients back-propagation.

It can be seen from Fig. 3, Eqs. 1 and 2 that the input feature map can be down-sampled without losing any feature information by 2D adaptive lifting scheme. Finally, **LL** $\in \mathrm{R}^{(C,H/2,W/2)}$, **LH** $\in \mathrm{R}^{(C,H/2,W/2)}$, **HL** $\in \mathrm{R}^{(C,H/2,W/2)}$, and **HH** $\in \mathrm{R}^{(C,H/2,W/2)}$ are concatenated fed into a Conv3 $\times$ 3 convolutional layer to adaptively fuse the features of different wavelet sub-bands.

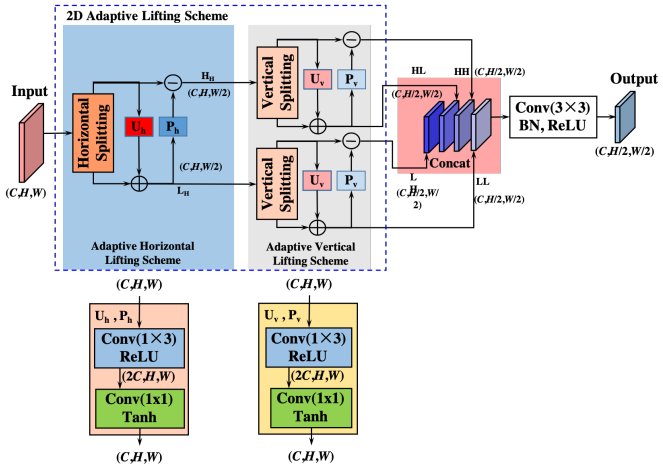


Fig. 3. The framework of adaptive wavelet down-sampling module. In AWDS module, we adopt 2D adaptive lifting scheme to perform multi-resolution wavelet transform on the input feature maps **Input** $\in \mathrm{R}^{(C,H,W)}$ to generate four wavelet sub-bands feature maps (**LL** $\in \mathrm{R}^{(C,H/2,W/2)}$, **LH** $\in \mathrm{R}^{(C,H/2,W/2)}$, **HL** $\in \mathrm{R}^{(C,H/2,W/2)}$, and **HH** $\in \mathrm{R}^{(C,H/2,W/2)}$), and a Conv3$\times$3 operation is used to fuse the features of different sub-bands to achieve down-sampling without any feature loss.

## 3.3 The adaptive multi-scale transformer module

As shown in Fig. 1, retinal edema lesions often co-occur in multiple morphologies, and as the disease progresses, the same symptom lesion usually shows serious scale differences in different OCT slices. Therefore, it is crucial for improving the segmentation performance to enhance the model's capacity to learn the global features of the retinal

edema lesions with different scales. Transformer, with an excellent ability to model long-range dependent features, has been applied in many fields of computer vision. Therefore, inspired by transformer, as shown in Fig. 4, dedicated to exploring multi-scale global long-dependent feature modeling in retinal OCT images, we propose a novel AMsTrans module. It can be seen from Fig. 2 and Fig. 4 that, different from the common transformer which focuses on single scale-size features, the proposed AMsTrans module takes feature maps with different scale-size at different stages of encoder path as input. First, the feature maps from level-1 ($F_1$), level-2 ($F_2$), level-3 ($F_3$), and level-4 ($F_4$) are fed into a bilinear interpolation down-sampling module followed by a Conv3×3 layer to normalize the resolution and channels to the top layer feature map ($F_T$). Then, the normalized feature maps and the top layer feature map are respectively fed into the corresponding scale dot-product block, so as to learn the long-dependent global features in different scale-size. This process can be analogized to the multi-head self-attention operation in the common transformer structure, i.e, the scale dot-product attention block of each scale-size feature map branch represents the SA head of multi-head self-attention in the common transformer. Meanwhile, inspired by an artificial neuron(AN) [47], the weighted sum operation followed by the Conv3×3 feature fusion layer is adopted to adaptively fuse long-dependent global features from multi-scale feature maps,

$$F_{Ms} = Conv3\times 3\left(\mathbf{1} * F_T + \sum_{i=1}^{4} w_i F_i\right), \tag{3}$$

where $\mathbf{1}$ is analogized to the bias in AN, while $w_i$ is the learnable weights obtained by Conv1×1 followed by Sigmoid normalization layer, as shown in Fig. 4,

$$W = \text{Sigmoid}\left(Conv1\times 1\left(\text{Concat}\left(F_T, F_1, F_2, F_3, F_4\right)\right)\right) \tag{4}$$

where $B$, $H$, and $W$ are the batch size, height, and width of the feature maps, respectively. Finally, the residual architecture is constructed by summing $F_T$ with $F_{Ms}$ to further enhance the model's ability to model strong semantic abstract features contained in the top layer, while avoiding the gradient vanishing. Different from previous multi-scale approaches [8], [29]–[31], our proposed AMsTrans module adaptively weight the global features learned from multiple scale-size feature maps, which can enhance the model's ability to represent the multi-scale global features for the different retinal lesions, while avoiding the interference of the weak semantic information of the shallow layer on the high-level semantic features contained in the top layer.

### 3.4 Uncertainty-aware segmentation head

How to make the segmentation result more reliable without losing the accuracy is significant for the joint segmentation of retinal edema lesions from OCT images. To this end, as shown in Fig. 2 and Fig. 5, we introduce an uncertainty-aware segmentation head based on subjective logic evidence uncertainty theory, which can generate retinal edema lesion segmentation results with corresponding uncertainty assessment map based on the feature evidence from the last layer of the main segmentation framework. Specifically, assuming

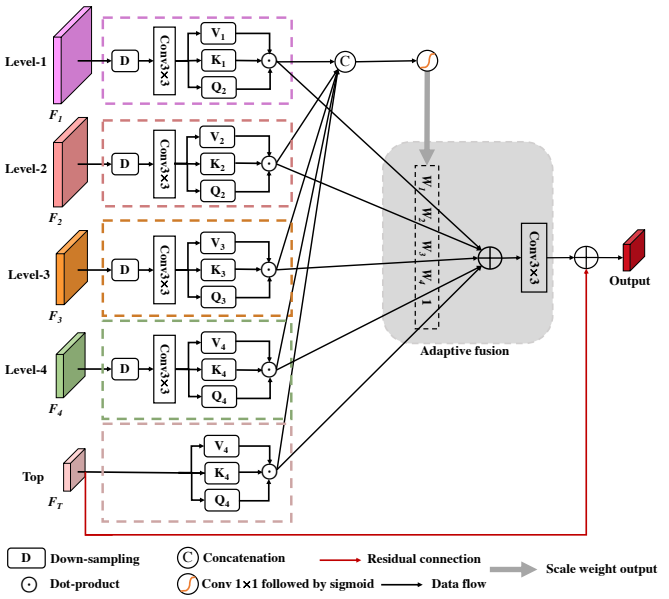


Fig. 4. Illustration of adaptive multi-scale transformer module. Our proposed AMsTrans module takes feature maps with different scale-size at different stages of encoder path as input. First, the feature maps from level-1 ($F_1$), level-2 ($F_2$), level-3 ($F_3$), and level-4 ($F_4$) are fed into a bilinear interpolation down-sampling module followed by a Conv3×3 layer to normalize the resolution and channels to the top layer feature map ($F_T$). Then, the normalized feature maps and the top layer feature map are respectively fed into the corresponding scale dot-product attention block, so as to learn the long-dependent global features in different scale-size. Meanwhile, inspired by an artificial neuron, the weighted sum operation followed by the Conv3×3 feature fusion layer is adopted to adaptively fuse long-dependent global features from multi-scale feature maps, where the weights are obtained by Conv1×1 followed by Sigmoid normalization layer.

there is a $K$-target segmentation task with $K$+1 mass maps, including $K$ belief mass maps corresponding to the target lesions and an overall uncertainty mass map, which are all non-negative and the values of the sum of the same coordinates to 1, *i.e.*, $u_{i,j} + \sum_{k=1}^{K} b_{i,j}^k = 1$, where $b_{i,j}^k \geq 0$ and $u_{i,j} \geq 0$ are the probability of the $k$-th target lesion at coordinate $(i, j)$ and the corresponding overall uncertainty score, respectively. In this paper, the joint segmentation of retinal edema lesions is a 3-target segmentation task, thus the $K$ is set to 3 in this paper. As shown in Fig. 5, the belief masses and overall uncertainty scores can be calculated by the following three steps:

**Step ① :** Obtaining the evidence $E_{i,j} = [e_{i,j}^1, e_{i,j}^2, ..., e_{i,j}^K]$ of three retinal edema lesions by applying *Softplus* activation function to ensure the feature values are larger than 0:

$$E = Softplus\left(F_{Out}\right) \in R^{B,K,H,W}, \tag{5}$$

where $F_{Out}$ is the final feature maps obtained from the final layer of our proposed segmentation backbone, while $B$,$H$, and $W$ indicate the batch size, height, and width of the $F_{Out}$, respectively.

**Step ② :** Parameterizing $E$ to Dirichlet distribution, as:

$$\boldsymbol{\alpha}_{i,j} = E_{i,j} + 1,\ i.e.,\ \alpha_{i,j}^k = e_{i,j}^k + 1, \tag{6}$$

where $\alpha^k$ and $e^k$ are the $k$-th category Dirichlet distribution parameters and evidence, respectively.

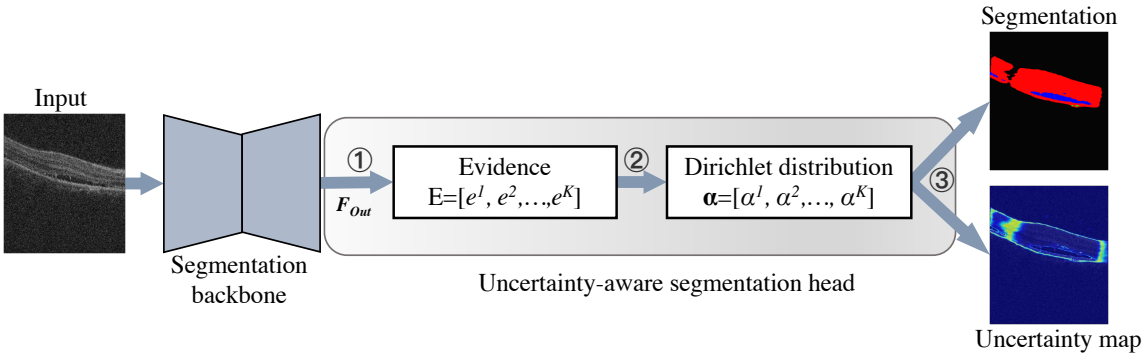


Fig. 5. Overview of uncertainty-aware segmentation head. Step ① : Obtaining the evidence $E$ of three retinal edema lesions by applying Softplus activation function to ensure the feature values are larger than 0; Step ② : Parameterizing $E$ to Dirichlet distribution; Step ③ : Calculating the belief masses and corresponding uncertainty scores.

**Step ③ :** Calculating the belief masses and corresponding uncertainty scores as:

$$b_{i,j}^k = \frac{e_{i,j}^k}{S} = \frac{\alpha_{i,j}^k - 1}{S},\ u_{i,j} = \frac{K}{S}, \tag{7}$$

where $S = \sum_{k=1}^{K}\left(e_{i,j}^k + 1\right) = \sum_{k=1}^{K}\alpha_{i,j}^k$ is the Dirichlet intensities. It can be seen from Eq. (7), the probability assigned to category $k$ is proportional to the observed evidence for category $k$. Conversely, if less total evidence is obtained, the greater the total uncertainty. The belief assignment can be considered as a subjective opinion. Given an opinion, the probability of $k$-th target lesion at $(i,j)$ coordinates is computed as $p_{i,j}^k = \frac{\alpha_{i,j}^k}{S}$ based on the Dirichlet distribution [48].

### 3.5 Loss function

In previous segmentation studies, a joint loss function ($\ell_O$) consisting of cross-entropy loss ($\ell_{CE}$) and Dice loss ($\ell_{Dice}$) has been widely used for model optimization in segmentation tasks, as follows:

$$\ell_O = \ell_{CE} + \ell_{Dice}, \tag{8}$$

where

$$\begin{aligned}\ell_{CE} &= -\sum_{k=1}^{K}\sum\nolimits_{(i,j)} Y_{i,j}^k log\left(p_{i,j}^k\right),\\ \ell_{Dice} &= \sum_{k=1}^{K}\sum\nolimits_{(i,j)}\left(1 - \frac{2Y_{i,j}^k p_{i,j}^k}{Y_{i,j}^k + p_{i,j}^k}\right),\end{aligned} \tag{9}$$

where $Y_{i,j}^k$ and $p_{i,j}^k$ indicate the ground truth and segmentation result of $k$-th at $(i,j)$, respectively. However, in this paper, SL is adapted to associate the evidence feature for generating final segmentation results with the parameters of Dirichlet distribution, i.e, given the evidence feature of $E_{i,j} = \left[e_{i,j}^1, e_{i,j}^2, ..., e_{i,j}^K\right]$, the Dirichlet distribution parameter $\boldsymbol{\alpha}_{i,j} = E_{i,j} + 1$ and the target lesion probabilities of $P_{i,j} = \left[p_{i,j}^1, p_{i,j}^2, ..., p_{i,j}^K | \boldsymbol{\alpha}\right]$ are obtained. Therefore, to guide the model optimization in the pixel level, the cross-entropy loss is re-formalized as follows:

$$\begin{aligned}\ell_{UCE} &= \int -\sum_{k=1}^{K}\sum\nolimits_{(i,j)} Y_{i,j}^k log\left(p_{i,j}^k\right)\frac{1}{B\left(\alpha_{i,j}\right)}\prod_{k=1}^{K}\left(p_{i,j}^k\right)^{\alpha_{i,j}^k - 1}\\ &= \sum_{k=1}^{K}\sum\nolimits_{(i,j)} Y_{i,j}^k\left(\psi\left(S_{i,j}\right) - \psi\left(\alpha_{i,j}^k\right)\right),\end{aligned} \tag{10}$$

where $\psi(\cdot)$ denotes the digamma function, while $B\left(\alpha_{i,j}^k\right)$ is the multinomial beta function for the concentration parameter of $k$-th target lesion $\alpha^k$ at $(i,j)$. Meanwhile, we further introduce the KL divergence function to ensure that incorrect labels will yield less evidence:

$$\begin{aligned}\ell_{KL} = &\log\left(\frac{\Gamma\left(\sum_{k=1}^{K}\sum_{(i,j)}\left(\tilde{\alpha}_{i,j}^k\right)\right)}{\Gamma(K)\sum_{k=1}^{K}\sum_{(i,j)}\Gamma\left(\tilde{\alpha}_{i,j}^k\right)}\right)\\ &+\sum_{k=1}^{K}\sum\nolimits_{(i,j)}\left(\tilde{\alpha}_{i,j}^k - 1\right)\left[\sum\nolimits_{(i,j)}\Phi\left(\tilde{\alpha}_{i,j}^k\right) - \Phi\left(\sum_{i=1}^{K}\sum\nolimits_{(i,j)}\tilde{\alpha}_{i,j}^k\right)\right],\end{aligned} \tag{11}$$

where $\Gamma(\cdot)$ is the gamma function, while $\tilde{\boldsymbol{\alpha}}_{i,j} = Y_{i,j} + (1 - Y_{i,j}) \odot \boldsymbol{\alpha}_{i,j}$ denotes the adjusted parameters of the Dirichlet distribution which aims to avoid penalizing the evidence of the ground-truth class to 0. Therefore, the objective function for the model optimization in pixel level based on the feature distribution parameterized by Dirichlet concentration is as follows:

$$L_{Un} = L_{UCE} + \lambda_u * L_{KL}, \tag{12}$$

where $\lambda_u$ is the balance factor weighted to $\ell_{KL}$. To prevent the model from focusing too much on KL loss at the early stage of training, which may lead to a poor exploration of the parameter space and result in a flat uniform distribution of the model's output, we initialize $\lambda_u$ as 0 and gradually increase it with the number of training iterations.

Meanwhile, we also propose a new type of uncertainty-aware loss function based on the dice loss function, aiming to guide the model optimization at the image level, as follows:

$$\begin{aligned}\ell_{U-Dice} = &\sum_{k=1}^{K}\sum\nolimits_{(i,j)}\left(1 - \frac{2Y_{i,j}^k p_{i,j}^k}{Y_{i,j}^k + p_{i,j}^k}\right)\\ &+\left(1 - \sum\nolimits_{(i,j)}\left(\frac{2\bar{Y}_{i,j}U_{i,j}}{\bar{Y}_{i,j} + U_{i,j}}\right)\right).\end{aligned} \tag{13}$$

where, $\bar{Y}_{i,j}$ represents the ground truth used to guide the model to assign high uncertainty scores to incorrectly segmented regions during training.

$$\begin{aligned}\bar{Y}_{i,j} &= 1 - \mathbf{1}\left\{P_{i,j}, Y_{i,j}\right\}, where\\ \mathbf{1}\left\{P_{i,j}, Y_{i,j}\right\} &= \begin{cases}1 & if\ P_{i,j} = Y_{i,j}\\ 0 & otherwise\end{cases}.\end{aligned} \tag{14}$$

As can be seen from Eq. 13 and Eq. 14, our proposed uncertainty-aware dice loss can not only guide the model to focus on the accuracy of lesion region segmentation, but also enable the model to assign high uncertainty scores to incorrectly segmented regions. Overall, in this paper, the objective function for model optimization is calculated as:

$$\ell_{overall} = \ell_{Un} + \ell_{U-Dice}. \tag{15}$$

As shown in Eq. 15, $\ell_{Un}$ is employed to guide the model optimization in pixel level, while the uncertainty-aware Dice loss $\ell_{U-Dice}$ is used to optimize the model in image level.

## 4 Experiments and Results

### 4.1 Dataset and implementation detail

We systematically evaluate the proposed method on the public database of AI-Challenge 2018 for retinal edema lesions segmentation, including the segmentation of retina edema(RE), sub-retinal fluid(SRF), and pigment epithelial detachment(PED) with severely imbalanced regional proportions. The regional ratio of RE, SRF, and PED in this database is counted as 0.8441:0.1493:0.0066, where the proportion of PED is much smaller than RE and SRF, which poses a great challenge to accurate segment PED lesion. The dataset contains 85 retinal OCT cubes (1024×512×128) with ground truth. We randomly divide the dataset into three exclusive subsets for training, validation, and testing based on 3D cubes with a ratio of 6:2:2. Therefore, the training dataset contains 6528 B-Scan OCT images, while validation and testing contain 2176 B-Scan OCT images, respectively. In addition, to comprehensively evaluate the performance of different methods, three indicators of Jaccard coefficient, Dice similarity index, and Accuracy (ACC) are used to quantitatively analyze the segmentation results from different methods.

For data preprocessing, we resize the retinal OCT B-Scan to 512×256 to improve the computational efficiency, while avoiding excessive detail loss and maintaining the average aspect ratio. To ensure fairness, all experiments involved in this paper were performed on the public platform Pytorch and RTX3090 GPU (24G). All networks are optimized by Adam with a batch size of 8 and maximum training epochs of 100. The initial learning rate and weight decay were set to 0.0005 and 0.0001, respectively.

### 4.2 Comparison results

As shown in Table 1, in order to comprehensively evaluate the performance of the proposed method, we compared with other excellent segmentation methods in including CNN-based models [5]–[8], [22], [49], [50], transformer-based networks [11], [12], and uncertainty-based approaches [42], [51]. It can be seen from Table 1 that the proposed method achieves the highest performance on all segmentation targets with average Jaccard, Dice, and Acc achieving 0.821, 0.896, and 0.970, respectively. Seen from Table 1, since both Ce-Net [7] and CPFNet [8] adopted the original pre-trained ResNet [17] as the feature extract network to capture rich feature information in medical images. However, the down-sampling operation in ResNet may cause feature loss for small targets, resulting in its performance degradation in our retinal edema lesion segmentation tasks with sparse and complex feature information. In addition, GLFRNet [50] improves the segmentation performance by introducing two modules of the global feature reconstruction module and the local feature reconstruction module, however, the problem of feature loss caused by the down-sampling still affects the performance for segmenting the PED lesions with very small regional proportions. Compared with these CNN-based methods, the transformer-based methods of TransUNet [11] and MsTGANet [22], both improve the segmentation performance by combining transformer with CNN to improve the model's ability to learn long-range dependent global features. As shown in Table 1, both TransUNet [11] and MsTGANet [22] achieve comparable performance with most CNN-based methods. In contrast to these CNNs-based and Transformer-based approaches, our proposed method alleviates feature loss and improves the ability to capture multi-resolution local features through our designed wavelet-enhanced feature extractor network, and further improves the model's capacity to capture multi-scale long-range dependent global features of retinal edema lesion by combining the proposed AMsTrans module with wavelet-enhanced extractor. Meanwhile, we also introduce a novel uncertainty-aware segmentation head to generate segmentation results with corresponding uncertainty evaluation maps, which enables our proposed method more reliable with higher segmentation accuracy. Therefore, as seen from Table 1, whether it is a PED with a small area proportion, an SRF with a clear boundary but a large scale variance, or an RE with a blurred boundary and a large area proportion, our proposed method achieves higher segmentation metrics for all these retinal edema lesions. The Jaccard of PED, SRF, and RE are improved by 20.6%, 1.5%, and 1.0% than GLFRNet [50], which achieves the highest average performance in all comparison methods. Meanwhile, we also compare our proposed method with the other excellent uncertainty-based approaches, such as Bayesian-based method [42] and TBraTS [51]. As shown in Table 2, our proposed method achieves better segmentation performance, and the average of Jaccard the proposed method improves by 2.5% and 2.4% over the Bayesian-based method and TBraTS, respectively. In addition, Fig.6 shows the segmentation results from different methods. As shown in Fig.6, the proposed method obtains better segmentation results than other models, the over-segmentation and missing-segmentation problems are significantly alleviated, especially for the PED lesion(Fig.6(c) and Fig.6(d)). These quantitative and qualitative analysis results show that our proposed method can significantly improve the joint segmentation performance of retinal edema lesions from OCT images, demonstrating the effectiveness of our proposed method.

### 4.3 Ablation study

We conducted a variety of ablation studies to demonstrate the effectiveness of the proposed method, the results are shown in Table 2. Here, the modified U-shaped network which adopted pre-trained ResNet as the extractor network is employed as the 'Backbone' model. It can be seen from

TABLE 1
The Jac and Dsc of different methods(Mean±Std)

| Methods | Jaccard | | | Average | Dice | | | Average | Acc | | | Average |
|---|---|---|---|---|---|---|---|---|---|---|---|---|
| | PED | SRF | RE | | PED | SRF | RE | | PED | SRF | RE | |
| UNet | 0.603 | 0.893 | 0.783 | 0.759 | 0.696 | 0.940 | 0.872 | 0.836 | 0.998 | 0.993 | 0.906 | 0.966 |
| AttUNet | 0.661 | 0.839 | 0.766 | 0.755 | 0.772 | 0.896 | 0.863 | 0.844 | 0.998 | 0.988 | 0.894 | 0.960 |
| CE-Net | 0.474 | 0.885 | 0.778 | 0.712 | 0.585 | 0.936 | 0.870 | 0.797 | 0.997 | 0.993 | 0.901 | 0.964 |
| CPFNet | 0.571 | 0.888 | 0.787 | 0.749 | 0.681 | 0.936 | 0.875 | 0.831 | 0.998 | 0.993 | 0.907 | 0.966 |
| UNet++ | 0.583 | 0.888 | 0.787 | 0.753 | 0.695 | 0.937 | 0.874 | 0.835 | 0.998 | 0.993 | 0.909 | 0.967 |
| GLFRNet | 0.630 | 0.888 | 0.794 | 0.771 | 0.739 | 0.936 | 0.880 | 0.852 | 0.998 | 0.994 | 0.909 | 0.967 |
| TransUNet | 0.611 | 0.887 | 0.776 | 0.758 | 0.718 | 0.938 | 0.870 | 0.842 | 0.998 | 0.993 | 0.901 | 0.964 |
| UTNet | 0.450 | 0.864 | 0.710 | 0.675 | 0.571 | 0.923 | 0.820 | 0.771 | 0.996 | 0.991 | 0.876 | 0.954 |
| MsTGANet | 0.629 | 0.889 | 0.782 | 0.767 | 0.742 | 0.937 | 0.871 | 0.850 | 0.998 | 0.993 | 0.906 | 0.966 |
| Bayesian | 0.723 | 0.888 | 0.792 | 0.801 | 0.817 | 0.937 | 0.879 | 0.878 | **0.999** | 0.993 | 0.910 | 0.967 |
| TBraTS | 0.721 | 0.890 | 0.793 | 0.802 | 0.820 | 0.938 | 0.879 | 0.879 | **0.999** | 0.993 | 0.911 | 0.968 |
| **Proposed** | **0.760** | **0.901** | **0.802** | **0.821** | **0.856** | **0.947** | **0.885** | **0.896** | **0.999** | **0.995** | **0.917** | **0.970** |

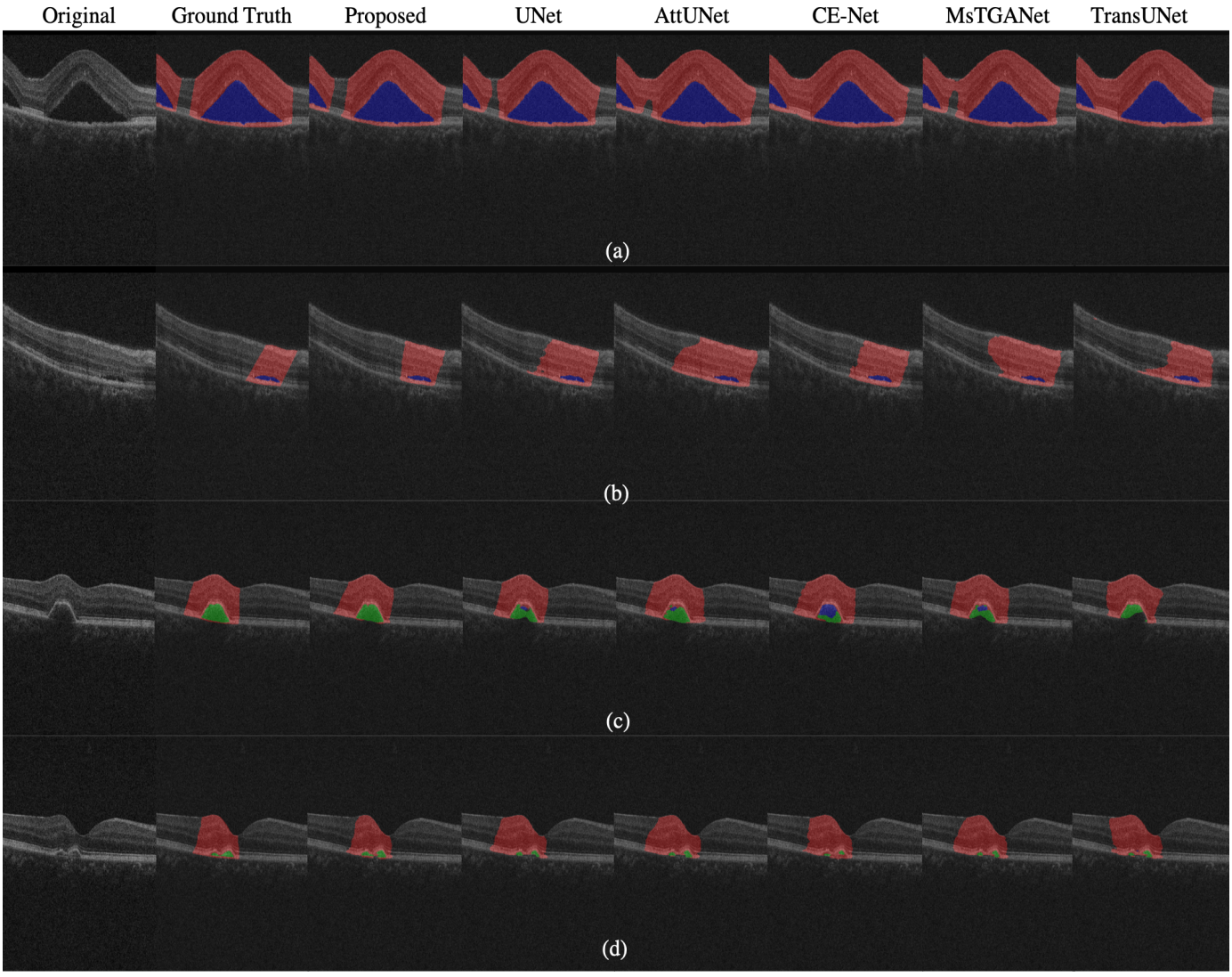


Fig. 6. Segmentation results of different models, where red represents RE, blue is SRF, and green indicates PED.

Table 2 that the model that adopted the proposed wavelet-enhanced extractor network achieves better segmentation performance than the Backbone model, especially for the tiny PED lesion, the Jaccard and Dice are improved by 9.6% and 5.23%, respectively. Furthermore, Fig. 7 shows the feature reconstruction results of different sub-bands generated by the lifting scheme at different levels. The feature reconstruction results of different sub-bands are very similar to traditional wavelet transform. As shown in Fig. 7 that the retinal structure information at different

TABLE 2
The Jac and Dsc of different methods(Mean±Std)

| Wavelet | AMsTrans | Uncertainty | Jaccard | | | Average | Dice | | | Average | ACC | | | Average |
|---|---|---|---|---|---|---|---|---|---|---|---|---|---|---|
| | | | PED | SRF | RE | | PED | SRF | RE | | PED | SRF | RE | |
| / | / | / | 0.604 | 0.882 | 0.779 | 0.755 | 0.726 | 0.935 | 0.870 | 0.844 | 0.998 | 0.992 | 0.904 | 0.965 |
| ✓ | / | / | 0.662 | 0.888 | 0.793 | 0.781 | 0.764 | 0.937 | 0.880 | 0.860 | 0.998 | 0.993 | 0.907 | 0.966 |
| ✓ | ✓ | / | 0.725 | 0.888 | 0.793 | 0.802 | 0.818 | 0.937 | 0.879 | 0.878 | **0.999** | 0.993 | 0.910 | 0.967 |
| ✓ | ✓ | ✓ | **0.760** | **0.901** | **0.802** | **0.821** | **0.856** | **0.947** | **0.885** | **0.896** | **0.999** | **0.995** | **0.917** | **0.970** |

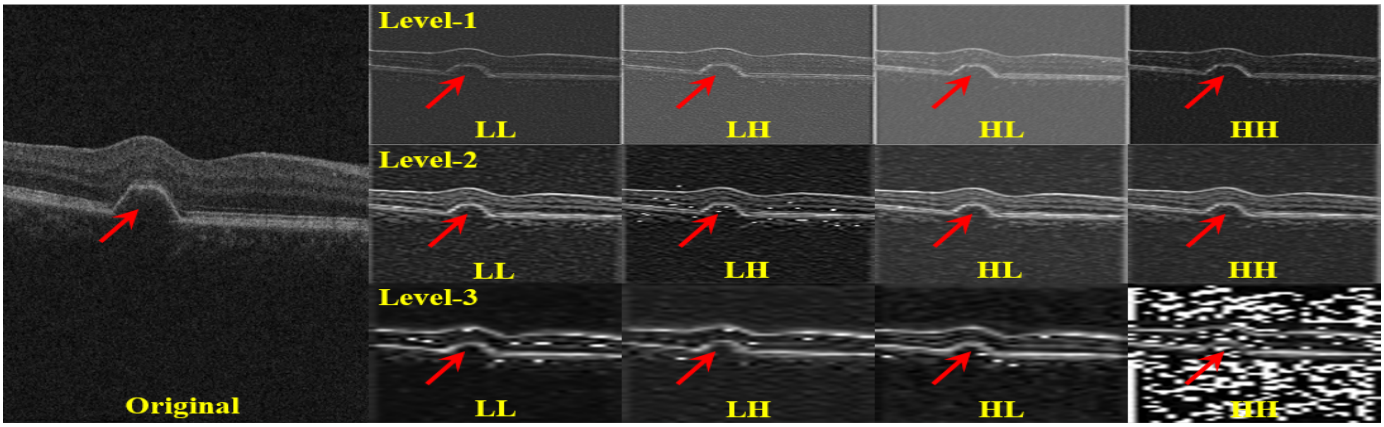


Fig. 7. Wavelet feature representation visualization. Red arrows indicate PED lesions. The retinal structure information at different levels of the feature extractor network is preserved and enhanced, especially for the PED lesion with small-size features.

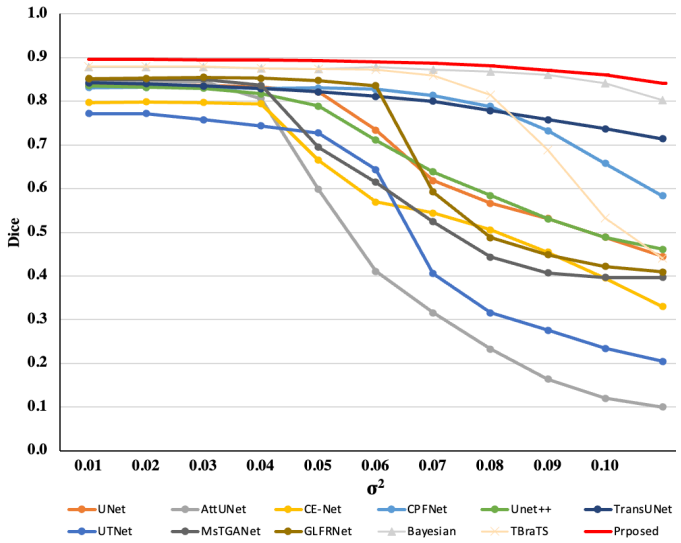


Fig. 8. Variation curve of Dice index with noise intensity for different methods. We can observe the interesting fact that the performance of all comparison methods decreases as the level of added noise increases, instead, our proposed method can still maintain higher segmentation performance than other excellent segmentation models and uncertainty approaches, which demonstrates that our proposed method can achieve higher segmentation accuracy with better robustness.

levels of the feature extractor network is preserved and enhanced, especially for the PED lesion with small-size features. The reconstruction results show that our proposed wavelet-enhanced feature extractor network (Wavelet in Table 2) can generate a wavelet representation to avoid feature loss while enhancing the ability of the network to represent local multi-resolution detailed features. Meanwhile, the average Jaccard of Wavelet+AMsTrans also improved by 6.2% and 2.7% to the Backbone model and Wavelet model, respectively, which demonstrates that the segmentation performance can be further improved by combining AMsTrans with Wavelet, proving the effectiveness of the AMsTrans module. Finally, the proposed method (Wavelet+AMsTrans+Uncertainty) achieves the highest metrics in all retinal edema lesions segmentation, especially the Jaccard of PED, which is 25.8% higher than the Backbone. In general, these ablation experimental results demonstrate the effectiveness of the components of our proposed method.

### 4.4 The reliability analysis

We also conducted experiments to further verify the reliability of our proposed method. As we know, speckle noise is the main cause of poor OCT image quality [3], [52], [53]. Therefore, we degraded the OCT image quality by adding Gaussian noise with different variances $\sigma^2$ to the original OCT image. As shown in Fig.8, we can observe the interesting fact that the performance of all comparison methods decreases as the level of added noise increases, instead, our proposed method can still maintain higher segmentation performance than other excellent segmentation models and uncertainty approaches, which demonstrates that our proposed method can achieve higher segmentation accuracy with better robustness. Meanwhile, Fig. 9 shows the segmentation results of the proposed method for noisy OCT images. As shown in Fig. 9, the histogram distribution between the original and noisy images changed significantly. Meanwhile, the quality of noisy images was degraded compared with the original OCT images, and the boundary information of retinal lesions in noisy images is more blurred, which is the main reason for the degraded segmentation performance of all methods. But our proposed method can provide the corresponding uncertainty evaluation, which makes the segmentation results more reliable. As shown in Fig. 9, although our proposed method presents incorrect segmentation results for noisy images, it also assigns high uncertain scores in the corresponding uncertainty map to

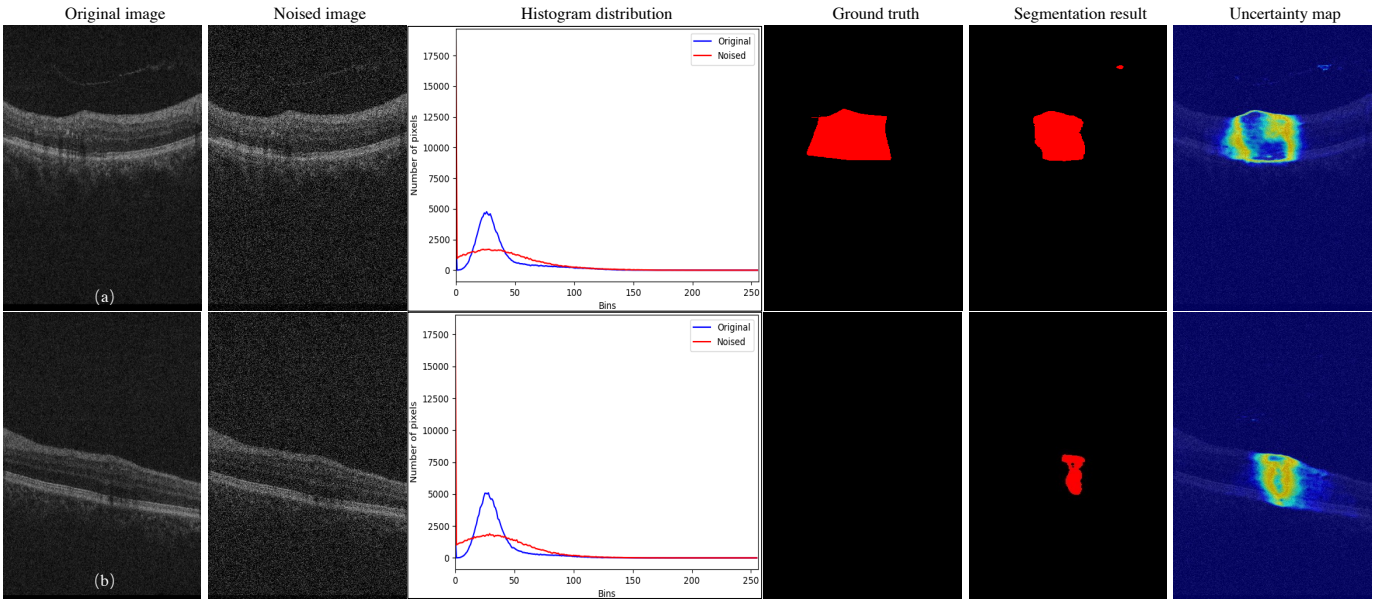


Fig. 9. The segmentation results of the proposed method for noise OCT images. Where regions with high uncertainty scores indicate that the segmentation result in that region may be incorrect and may require a double-check by the physician, while regions with low certainty scores indicate a high level of confidence in the segmentation result.

reflect the low confidence for the segmentation results, i.e, it implicitly indicates that the segmentation regions with high uncertainty scores may be unreliable and need to be double-checked by the ophthalmologist, which makes our proposed method more reliable and potentially avoid disasters from OOD samples.

## 5 Conclusion and Discussion

In this paper, focusing on the challenges in the task of retinal edema lesions joint segmentation from OCT images, we propose a novel reliable multi-scale wavelet enhanced transformer network by integrating CNN, wavelet transform, transformer concept, and uncertainty mechanism. To our best knowledge, it is the first work aiming to develop a reliable segmentation method for retinal edema lesions joint segmentation from OCT images. We conducted comprehensive experiments on AI-Challenge 2018 dataset for retinal edema lesions joint segmentation to validate our proposed method. The experimental results show that our proposed method achieves better segmentation performance with higher robustness than other state-of-the-art segmentation approaches. Meanwhile, unlike previous segmentation methods, our proposed method can produce reliable segmentation results with an estimated uncertainty without loss of accuracy, which makes our proposed model more reliable.

Our proposed method achieves promising performance on the challenging task of retinal edema lesions joint segmentation from OCT images. However, there are still the following issues to be further explored: 1) To further verify the performance on datasets with large variances in data distribution, such as data collected from different OCT acquisition scanners with different modes. Therefore, in our future work, we will collect more data with retinal edema lesions from different OCT scanners and acquisition modes to build a larger and more comprehensive database to further evaluate the performance of our proposed method. 2) Due to the complex pathological features, large morphological differences, and blurred boundaries of retinal edema lesions in retinal OCT images, it has always been a great challenge to annotate pixel-level labels for retinal edema lesions, which is time-consuming and expensive. Therefore, how to leverage a large amount of unlabeled data to further improve the performance of retinal edema lesions joint segmentation is a very meaningful research topic. Therefore, developing a semi/weakly supervised reliable segmentation method to further improve the performance of retinal edema lesions joint segmentation is also one of our future research works. In addition, we will continue to work on improving our proposed method to make it suitable for more complex medical image segmentation tasks.

## Acknowledgment

This work was supported by A*STAR Advanced Manufacturing and Engineering (AME) Programmatic Fund (A20H4b0141) and the Exploration Project of Natural Science Foundation of Zhejiang Province(LQ22F010003).

## References

[1] S. Wild, G. Roglic, A. Green, R. Sicree, and H. King, "Global prevalence of diabetes: estimates for the year 2000 and projections for 2030," *Diabetes care*, vol. 27, no. 5, pp. 1047–1053, 2004.

[2] D. Huang, E. A. Swanson, C. P. Lin, J. S. Schuman, W. G. Stinson, W. Chang, M. R. Hee, T. Flotte, K. Gregory, C. A. Puliafito *et al.*, "Optical coherence tomography," *science*, vol. 254, no. 5035, pp. 1178–1181, 1991.

[3] X. Xi, X. Meng, Z. Qin, X. Nie, Y. Yin, and X. Chen, "Ia-net: informative attention convolutional neural network for choroidal neovascularization segmentation in oct images," *Biomedical Optics Express*, vol. 11, no. 11, pp. 6122–6136, 2020.

[4] D. Xiang, H. Tian, X. Yang, F. Shi, W. Zhu, H. Chen, and X. Chen, "Automatic segmentation of retinal layer in oct images with choroidal neovascularization," *IEEE Transactions on Image Processing*, vol. 27, no. 12, pp. 5880–5891, 2018.

[5] O. Ronneberger, P. Fischer, and T. Brox, "U-net: Convolutional networks for biomedical image segmentation," in *International Conference on Medical image computing and computer-assisted intervention*. Springer, 2015, pp. 234–241.

[6] O. Oktay, J. Schlemper, L. L. Folgoc, M. Lee, M. Heinrich, K. Misawa, K. Mori, S. McDonagh, N. Y. Hammerla, B. Kainz *et al.*, "Attention u-net: Learning where to look for the pancreas," *arXiv preprint arXiv:1804.03999*, 2018.

[7] Z. Gu, J. Cheng, H. Fu, K. Zhou, H. Hao, Y. Zhao, T. Zhang, S. Gao, and J. Liu, "Ce-net: Context encoder network for 2d medical image segmentation," *IEEE transactions on medical imaging*, vol. 38, no. 10, pp. 2281–2292, 2019.

[8] S. Feng, H. Zhao, F. Shi, X. Cheng, M. Wang, Y. Ma, D. Xiang, W. Zhu, and X. Chen, "Cpfnet: Context pyramid fusion network for medical image segmentation," *IEEE transactions on medical imaging*, vol. 39, no. 10, pp. 3008–3018, 2020.

[9] A. Vaswani, N. Shazeer, N. Parmar, J. Uszkoreit, L. Jones, A. N. Gomez, Ł. Kaiser, and I. Polosukhin, "Attention is all you need," *Advances in neural information processing systems*, vol. 30, 2017.

[10] A. Dosovitskiy, L. Beyer, A. Kolesnikov, D. Weissenborn, X. Zhai, T. Unterthiner, M. Dehghani, M. Minderer, G. Heigold, S. Gelly *et al.*, "An image is worth 16x16 words: Transformers for image recognition at scale," *arXiv preprint arXiv:2010.11929*, 2020.

[11] J. Chen, Y. Lu, Q. Yu, X. Luo, E. Adeli, Y. Wang, L. Lu, A. L. Yuille, and Y. Zhou, "Transunet: Transformers make strong encoders for medical image segmentation," *arXiv preprint arXiv:2102.04306*, 2021.

[12] Y. Gao, M. Zhou, and D. N. Metaxas, "Utnet: a hybrid transformer architecture for medical image segmentation," in *International Conference on Medical Image Computing and Computer-Assisted Intervention*. Springer, 2021, pp. 61–71.

[13] Z. Liu, Y. Lin, Y. Cao, H. Hu, Y. Wei, Z. Zhang, S. Lin, and B. Guo, "Swin transformer: Hierarchical vision transformer using shifted windows," in *Proceedings of the IEEE/CVF International Conference on Computer Vision*, 2021, pp. 10 012–10 022.

[14] A. Krizhevsky, I. Sutskever, and G. E. Hinton, "Imagenet classification with deep convolutional neural networks," *Advances in neural information processing systems*, vol. 25, 2012.

[15] K. Simonyan and A. Zisserman, "Very deep convolutional networks for large-scale image recognition," *arXiv preprint arXiv:1409.1556*, 2014.

[16] C. Szegedy, W. Liu, Y. Jia, P. Sermanet, S. Reed, D. Anguelov, D. Erhan, V. Vanhoucke, and A. Rabinovich, "Going deeper with convolutions," in *Proceedings of the IEEE conference on computer vision and pattern recognition*, 2015, pp. 1–9.

[17] K. He, X. Zhang, S. Ren, and J. Sun, "Deep residual learning for image recognition," in *Proceedings of the IEEE conference on computer vision and pattern recognition*, 2016, pp. 770–778.

[18] S. Xie, R. Girshick, P. Dollár, Z. Tu, and K. He, "Aggregated residual transformations for deep neural networks," in *Proceedings of the IEEE conference on computer vision and pattern recognition*, 2017, pp. 1492–1500.

[19] J. Long, E. Shelhamer, and T. Darrell, "Fully convolutional networks for semantic segmentation," in *Proceedings of the IEEE conference on computer vision and pattern recognition*, 2015, pp. 3431–3440.

[20] J. Fu, J. Liu, H. Tian, Y. Li, Y. Bao, Z. Fang, and H. Lu, "Dual attention network for scene segmentation," in *Proceedings of the IEEE/CVF conference on computer vision and pattern recognition*, 2019, pp. 3146–3154.

[21] H. Zhao, J. Shi, X. Qi, X. Wang, and J. Jia, "Pyramid scene parsing network," in *Proceedings of the IEEE conference on computer vision and pattern recognition*, 2017, pp. 2881–2890.

[22] M. Wang, W. Zhu, F. Shi, J. Su, H. Chen, K. Yu, Y. Zhou, Y. Peng, Z. Chen, and X. Chen, "Mstganet: Automatic drusen segmentation from retinal oct images," *IEEE Transactions on Medical Imaging*, 2021.

[23] J. Devlin, M.-W. Chang, K. Lee, and K. Toutanova, "Bert: Pre-training of deep bidirectional transformers for language understanding," *arXiv preprint arXiv:1810.04805*, 2018.

[24] Z. Dai, Z. Yang, Y. Yang, J. Carbonell, Q. V. Le, and R. Salakhutdinov, "Transformer-xl: Attentive language models beyond a fixed-length context," *arXiv preprint arXiv:1901.02860*, 2019.

[25] Z. Yang, Z. Dai, Y. Yang, J. Carbonell, R. R. Salakhutdinov, and Q. V. Le, "Xlnet: Generalized autoregressive pretraining for language understanding," *Advances in neural information processing systems*, vol. 32, 2019.

[26] A. Srinivas, T.-Y. Lin, N. Parmar, J. Shlens, P. Abbeel, and A. Vaswani, "Bottleneck transformers for visual recognition," in *Proceedings of the IEEE/CVF conference on computer vision and pattern recognition*, 2021, pp. 16 519–16 529.

[27] D. Zhang, H. Zhang, J. Tang, M. Wang, X. Hua, and Q. Sun, "Feature pyramid transformer," in *European Conference on Computer Vision*. Springer, 2020, pp. 323–339.

[28] H. Cao, Y. Wang, J. Chen, D. Jiang, X. Zhang, Q. Tian, and M. Wang, "Swin-unet: Unet-like pure transformer for medical image segmentation," *arXiv preprint arXiv:2105.05537*, 2021.

[29] Y. Xie, J. Zhang, C. Shen, and Y. Xia, "Cotr: Efficiently bridging cnn and transformer for 3d medical image segmentation," in *International conference on medical image computing and computer-assisted intervention*. Springer, 2021, pp. 171–180.

[30] J. Wang, Z. Wu, J. Chen, and Y.-G. Jiang, "M2tr: Multi-modal multi-scale transformers for deepfake detection," *arXiv preprint arXiv:2104.09770*, 2021.

[31] Y. Zhang, J. Cao, L. Zhang, X. Liu, Z. Wang, F. Ling, and W. Chen, "A free lunch from vit: adaptive attention multi-scale fusion transformer for fine-grained visual recognition," in *ICASSP 2022-2022 IEEE International Conference on Acoustics, Speech and Signal Processing (ICASSP)*. IEEE, 2022, pp. 3234–3238.

[32] N. Chervyakov, P. Lyakhov, D. Kaplun, D. Butusov, and N. Nagornov, "Analysis of the quantization noise in discrete wavelet transform filters for image processing," *Electronics*, vol. 7, no. 8, p. 135, 2018.

[33] N. Sathiyanathan, "Medical image compression using view compensated wavelet transform," *Journal of Global Research in Computer Science*, vol. 9, no. 9, pp. 01–04, 2018.

[34] A. A. Abdulrahman, M. Rasheed, and S. Shihab, "The analytic of image processing smoothing spaces using wavelet," in *Journal of Physics: Conference Series*, vol. 1879, no. 2. IOP Publishing, 2021, p. 022118.

[35] S. Fujieda, K. Takayama, and T. Hachisuka, "Wavelet convolutional neural networks," *arXiv preprint arXiv:1805.08620*, 2018.

[36] T. Williams and R. Li, "Advanced image classification using wavelets and convolutional neural networks," in *2016 15th IEEE international conference on machine learning and applications (ICMLA)*. IEEE, 2016, pp. 233–239.

[37] M. X. B. Rodriguez, A. Gruson, L. Polania, S. Fujieda, F. Prieto, K. Takayama, and T. Hachisuka, "Deep adaptive wavelet network," in *Proceedings of the IEEE/CVF Winter Conference on Applications of Computer Vision*, 2020, pp. 3111–3119.

[38] G. Huang, Z. Liu, L. Van Der Maaten, and K. Q. Weinberger, "Densely connected convolutional networks," in *Proceedings of the IEEE conference on computer vision and pattern recognition*, 2017, pp. 4700–4708.

[39] J. Denker and Y. LeCun, "Transforming neural-net output levels to probability distributions," *Advances in neural information processing systems*, vol. 3, 1990.

[40] D. J. MacKay, "A practical bayesian framework for backpropagation networks," *Neural computation*, vol. 4, no. 3, pp. 448–472, 1992.

[41] R. M. Neal, *Bayesian learning for neural networks*. Springer Science & Business Media, 2012, vol. 118.

[42] Y. Gal and Z. Ghahramani, "Dropout as a bayesian approximation: Representing model uncertainty in deep learning," in *international conference on machine learning*. PMLR, 2016, pp. 1050–1059.

[43] B. Lakshminarayanan, A. Pritzel, and C. Blundell, "Simple and scalable predictive uncertainty estimation using deep ensembles," *Advances in neural information processing systems*, vol. 30, 2017.

[44] M. Sensoy, L. Kaplan, and M. Kandemir, "Evidential deep learning to quantify classification uncertainty," *Advances in Neural Information Processing Systems*, vol. 31, 2018.

[45] J. Van Amersfoort, L. Smith, Y. W. Teh, and Y. Gal, "Uncertainty estimation using a single deep deterministic neural network," in *International conference on machine learning*. PMLR, 2020, pp. 9690–9700.

[46] Z. Han, C. Zhang, H. Fu, and J. T. Zhou, "Trusted multi-view classification," *arXiv preprint arXiv:2102.02051*, 2021.

[47] L. D. Harmon, "Artificial neuron," *Science*, vol. 129, no. 3354, pp. 962–963, 1959.

[48] B. A. Frigyik, A. Kapila, and M. R. Gupta, "Introduction to the dirichlet distribution and related processes," 2010.

[49] Z. Zhou, M. M. Rahman Siddiquee, N. Tajbakhsh, and J. Liang, "Unet++: A nested u-net architecture for medical image segmentation," in *Deep learning in medical image analysis and multimodal learning for clinical decision support*. Springer, 2018, pp. 3–11.

[50] J. Song, X. Chen, Q. Zhu, F. Shi, D. Xiang, Z. Chen, Y. Fan, L. Pan, and W. Zhu, "Global and local feature reconstruction for medical image segmentation," *IEEE Transactions on Medical Imaging*, 2022.
[51] K. Zou, X. Yuan, X. Shen, M. Wang, and H. Fu, "Tbrats: Trusted brain tumor segmentation," in *International Conference on Medical Image Computing and Computer-Assisted Intervention*. Springer, 2022, pp. 503–513.
[52] M. Wang, W. Zhu, K. Yu, Z. Chen, F. Shi, Y. Zhou, Y. Ma, Y. Peng, D. Bao, S. Feng *et al.*, "Semi-supervised capsule cgan for speckle noise reduction in retinal oct images," *IEEE Transactions on Medical Imaging*, vol. 40, no. 4, pp. 1168–1183, 2021.
[53] Y. Zhou, K. Yu, M. Wang, Y. Ma, Y. Peng, Z. Chen, W. Zhu, F. Shi, and X. Chen, "Speckle noise reduction for oct images based on image style transfer and conditional gan," *IEEE Journal of Biomedical and Health Informatics*, 2021.